Available online at www.sciencedirect.com
SCIENCE DIRECT®
Journal of Solid State Chemistry 170 (2003) 424–434
JOURNAL OF SOLID STATE CHEMISTRY
http://elsevier.com/locate/jssc

The oxycarbonates $Sr_4(Fe_{2-x}Mn_x)_{1+y}(CO_3)_{1-3y}O_{6(1+y)}$: nano, micro and average structural approach

Y. Bréard,[a] C. Michel,[a,*] M. Hervieu,[a] N. Nguyen,[a] F. Studer,[a] A. Maignan,[a] B. Raveau,[a] and F. Bourée[b]

[a] *Laboratoire CRISMAT, ISMRA, UMR-CNRS 6508, 6, Boulevard du Maréchal Juin, F14050 Caen Cédex, France*
[b] *LLB, CEA Saclay, 91191 Gif sur Yvette, France*

Received 25 June 2002; accepted 23 October 2002

Abstract

The possibility to synthesize layered oxycarbonates, with nominal composition $Sr_4Fe_{2-x}Mn_xO_6CO_3$ involving trivalent manganese, with $0 \leq x \leq 1.5$, is reported for the first time. The structural study of $Sr_4FeMnO_6CO_3$ using NPD, HREM, Mössbauer and XANES, shows that this phase is closely related to $n=3$ member of the Ruddlesden–Popper family. It derives from the latter by replacing the middle layer of transition metal octahedra by triangular CO_3 groups, with two different "flag" and "coat hanger" configurations. The magnetic order is antiferromagnetic and fundamentally different from the magnetic behavior of $Sr_4Fe_2O_6CO_3$.

1. Introduction

Intergrowth structures in inorganic systems have been a great source of solid-state chemical research for many years. The discovery of superconductivity in layered cuprates [1] and of giant magnetoresistance in layered manganites [2] has focused the attention on intergrowth structures based on perovskite blocks. One of the most famous is the Ruddlesden–Popper (RP) series [3] of composition $A_{n+1}M_nO_{3n+1}$ (where A is a rare earth, an alkaline or an alkaline-earth and M a transition metal). These compounds are built up from perovskite-like layers of corner sharing MO_6 octahedra which are n octahedra thick, separated by $(AO)_2$ rock salt layers. For the $n=3$ member of the RP series, $Sr_4M_3O_{10}$ (M = Fe, Cr), it has recently been shown that the MO_6 octahedra of the central layer of the triple perovskite slab can be replaced by triangular carbonate groups [4–6] leading to the $Sr_4M_2O_6CO_3$ family. Such an ability of the CO_3 groups to substitute for transition metal octahedra was also observed for other layered copper-based oxycarbonates [7,8]. In contrast to iron, chromium and copper, no manganese oxycarbonate with a layered structure is known to date, though Mn oxycarbonates with a tridimensional framework, such as $Sr_5Mn_4CO_3O_{10}$ [9] and $SrMn_{1-y}(B,C)_yO_{3-\delta}$ [10] were recently synthesized. In this paper we show that the possibility to form oxycarbonates in layered structures can be extended to manganese. We demonstrate that, in the new oxycarbonates $Sr_4(Fe_{2-x}Mn_x)_{1+y}(CO_3)_{1-3y}O_{6(1+y)}$ ($0 < x \leqslant 1.5$), manganese is trivalent and that the oxycarbonate groups adopt two configurations, "flag" and "coat hanger". The antiferromagnetic behavior of these phases, fundamentally different from that of $Sr_4Fe_2O_6CO_3$ is also evidenced.

2. Experimental

2.1. Synthesis

The different oxides with nominal composition $Sr_4Fe_{2-x}Mn_xO_6CO_3$ have been prepared from appropriate mixtures of Fe_2O_3, Mn_2O_3, SrO and $SrCO_3$ which were used as CO_2 source. The compounds were intimately mixed, pressed in the form of bars, introduced in evacuated silica tubes and heated up to 1200°C for 12 h. Heating and cooling down to room temperature were performed in 6 h. After thermal treatment, the products appeared as black sintered bars.

*Corresponding author. Fax: 31-95-16-00.
E-mail address: claude.michel@ismra.fr (C. Michel).

0022-4596/03/$ - see front matter © 2002 Elsevier Science (USA). All rights reserved.
doi:10.1016/S0022-4596(02)00135-4

2.2. Structural analysis

The electron diffraction (ED) investigation was carried out with a JEOL 200CX microscope, tilting around the crystallographic axes. The high-resolution electron microscopy (HREM) study was performed with a TOPCON 002B, operating at 200 kV and having a point resolution of 1.8 Å. Image calculations were carried out using the Mac Tempas program. Both microscopes are equipped with an energy dispersive spectroscopy (EDS) analyzer.

Sample purity was checked by X-ray diffraction using a PHILIPS vertical diffractometer PW1830 equipped with a secondary graphite monochromator and working with the Cu$K\alpha$ radiation. Data were collected by step scanning of 0.025° (2θ) over an angular range $5° < 2\theta < 120°$. X-ray diffraction patterns were used for lattice constant measurements.

Neutron powder diffraction data (for $Sr_4FeMnO_6CO_3$ sample) were collected at room temperature at LLB (Saclay-France) on the high-resolution 3T2 diffractometer, using the wavelength 1.2251 Å, in the angular range $6° < 2\theta < 126°$ with steps of 0.05° (2θ). The scattering lengths of the differents atoms were those included in the Rietveld profile analysis program package (FULLPROF [11]).

The X-ray absorption spectra at Mn and Fe K-edges were recorded at room temperature in a classical transmission mode at the EXAFS I station (channel cut the monochromator) using the synchrotron radiation of the DCI storage ring of LURE (Orsay) working at 1.85 GeV with a 250 mA current. The energy resolution at Mn K-edge is estimated at 1.3 eV whereas it is estimated at 1.2 eV for Fe K-edge, whereas the reproducibility of the monochromator is as good as 0.3 eV. The normalization procedure used throughout this work was a standard one: after subtraction of the same diffusion background on the XANES and EXAFS spectra, recorded in the same experimental conditions, a point located at an energy of 800 eV from the edge, where no more EXAFS oscillations were still observable, was set to unity. Then the intensity of a point with an energy between 50 and 100 eV from the edge was recorded on the EXAFS spectrum and reported on the XANES to set the normalization height.

2.3. Magnetism and mössbauer spectroscopy

Magnetic susceptibility $\chi(T)$ measurements were investigated in the range 5–300 K using a DC SQUID quantum design magnetometer (ZFCW method) with an applied G.

The ^{57}Fe Mössbauer spectrum at room temperature of the powdered $Sr_4FeMnO_6CO_3$ ($x=1$) sample was recorded in transmission mode using a conventional spectrometer operating in the constant acceleration mode. ^{57}Co/Rh was used as the γ-ray source. The isomer shift (IS) is referred to metallic iron.

3. Results and discussion

The series with nominal composition $Sr_4Fe_{2-x}Mn_xO_6CO_3$ was studied in the range $0 \leqslant x \leqslant 2$. As shown by the X-ray diffraction patterns (Fig. 1) and if one excepts $SrCO_3$ which is sometimes observed as minority phase in variable quantities, all samples can be considered as single phase for $x \leqslant 1.5$. It should be noted that the amount of $SrCO_3$ which appears for $x \geqslant 0.7$ and increases with x (Fig. 2), suggests compositional mod-

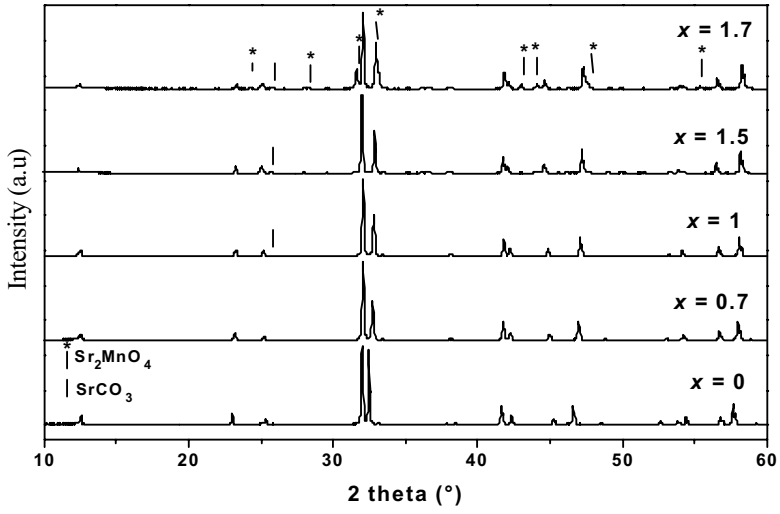

Fig. 1. X-ray powder diffraction pattern of some nominal compositions of $Sr_4Fe_{2-x}Mn_xO_6CO_3$. For $x=0.0$, 0.7, 1, 1.5 and 1.7, the main diffraction peak of $SrCO_3$ (stick) and Sr_2MnO_4 (stick and star) are observed.

ifications for high manganese content. For $x=1.7$, close to the limit composition ($x=1.5$), $SrCO_3$ and $Sr_2MnO_{4-\delta}$ were observed as secondary phases while for $x=2$ a mixture of $SrCO_3$, $Sr_2MnO_{4-\delta}$ and $Sr_5Mn_4O_{10}CO_3$ [9] was obtained.

Concerning the single phase samples ($x\leqslant 1.5$), the X-ray diffraction data are very close to those of $Sr_4Fe_2O_6CO_3$ [4] and can be indexed in the space group: $I4/mmm$ with cell parameters $a\approx 3.8\,\text{Å}=a_P$ and $c\approx 28\,\text{Å}$.The variation of the lattice constant as a function of the Mn substitution rate is plotted in Fig. 3. One can see a small and continuous decrease of a as x increases, whereas c increases. The decrease of a (1.2%) is approximately equal to the increase of c (1.4%), involving a decrease of the cell volume. These variations cannot be explained by the simple replacement of Fe^{3+} ion by Mn^{3+} ion which have same ionic radius.

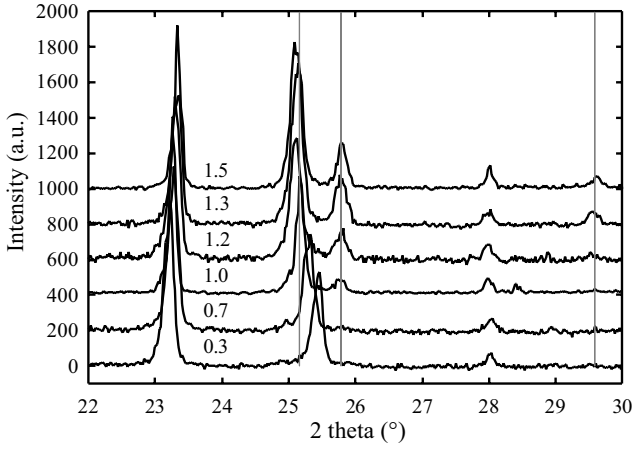

Fig. 2. Portion of X-ray diffraction patterns ($x=0.0$, 0.3, 0.7, 1, 1.2, 1.3 and 1.5) showing the evolution of the amount of $SrCO_3$ (vertical bars are the Bragg angle position of $SrCO_3$ diffraction peaks).

3.1. EDS study and oxygen content

The EDS analysis, performed on numerous crystallites for each composition, revealed that for $x<0.7$ the cationic formula $Sr_4Fe_{2-x}Mn_xO_6CO_3$ are, in the limit of the technique accuracy, in agreement with the nominal compositions. For $0.7\leqslant x\leqslant 1.5$ the ratio Fe/Mn remains close to the nominal one contrary to the ratio Sr/(Fe + Mn) which decreases as x increases (Table 1). This suggests that structural modifications could appear in the matrix, such as the formation of $n=3$ members of the RP family. A detailed HREM study (hereafter) has been performed in order to clarify this point.

Oxygen content was determined for several compositions, by redox back titration (RBT) using standard solutions of Fe^{2+} and potassium dichromate as described elsewhere [12]. For each analyzed sample, the oxygen content was found to be very close to that expected. This technique was preferred to the thermogravimetric analysis (TGA) which does not lead to well-known residues at high temperature (1200°C).

Table 1
Cationic formula deduced from EDS analysis, of the "$Sr_4Fe_{2-x}Mn_xO_6CO_3$" samples

x	Cationic formula (EDS) ± 0.03
0.3	$Sr_4Fe_{1.72}Mn_{0.28}$
0.7	$Sr_4Fe_{1.37}Mn_{073}$
1.0	$Sr_4Fe_{1.1}Mn_{1.09}$
1.3	$Sr_4Fe_{0.81}Mn_{1.52}$
1.5	$Sr_4Fe_{0.61}Mn_{1.79}$

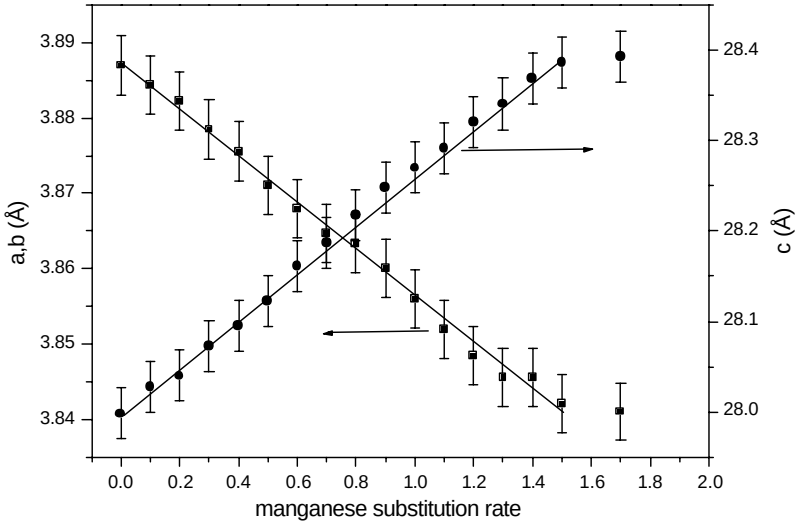

Fig. 3. Evolution of the lattice constants as a function of the manganese substitution rate x.

3.2. Microstructural state

3.2.1. ED study

Reconstructing the reciprocal space by tilting around the crystallographic axes confirms the cell parameters and shows that, whatever the composition, all the crystallites exhibit a system of intense reflections consistent with the $I4/mmm$ space group. Typical [0 0 1] and [0 1 0] ED patterns are given in Figs. 4a and b. In most of the crystallites, a second system of weak reflections is characterized by the presence of additional sharp spots in the [0 0 1] ED patterns at positions $\frac{1}{2}\frac{1}{2}0$ (white triangles in Fig. 5a). The reconstruction of the reciprocal space leads to a doubling of the cell: $a \approx b \approx a_p\sqrt{2}$ and the conditions of reflections ($hkl : k+l=2n$, $hk0 : (k=2n)$, $0kl : k=2n$ and $l=2n$, $h0l :$ (h=2n and l=2n)) are consistent with $Aba2$ space group. These additional spots are especially intense in the [3 $\bar{1}$ 0] ED patterns (indicated by white triangles in Fig. 5b) and scarcely visible along [0 1 0]. Viewing the crystals perpendicularly to the c^*-axis shows that these reflections are elongated, often resulting in diffuse streaky lines. The streaking of the superlattice reflections suggests disorder phenomena in successive layers, which have been characterized by HREM. This fact adding to the weakness and diffuse shape of these extra reflections make us to choose for neutrons or X-ray diffraction calculations, the space group $I4/mmm$ for the determination of the average structure.

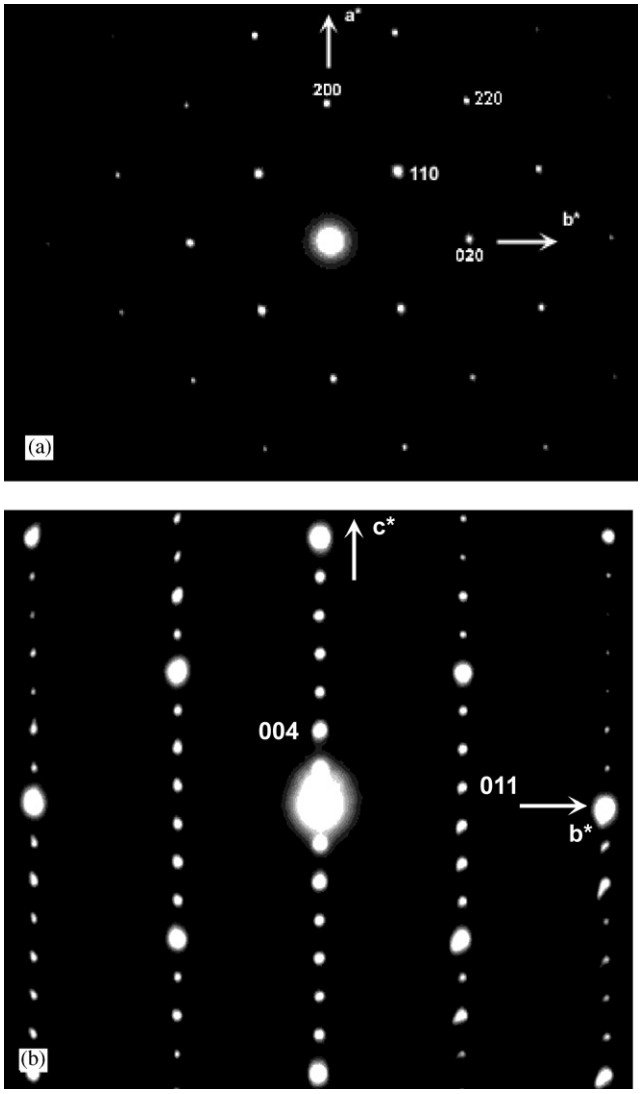

Fig. 4. (a) [001] and (b) [010] ED pattern of $Sr_4FeMnO_6CO_3$.

3.3. Average structure

3.3.1. $Sr_4FeMnO_6CO_3$, neutron diffraction study

The structure of these oxycarbonates has been studied by powder neutron diffraction for the nominal composition $Sr_4FeMnO_6CO_3$. Calculations were carried out in the space group $I4/mmm$. All the atoms, except those involved in the triangular carbonate group, were located according to previous structural studies [4,5], Fe and Mn sitting on the same crystallographic site. Three

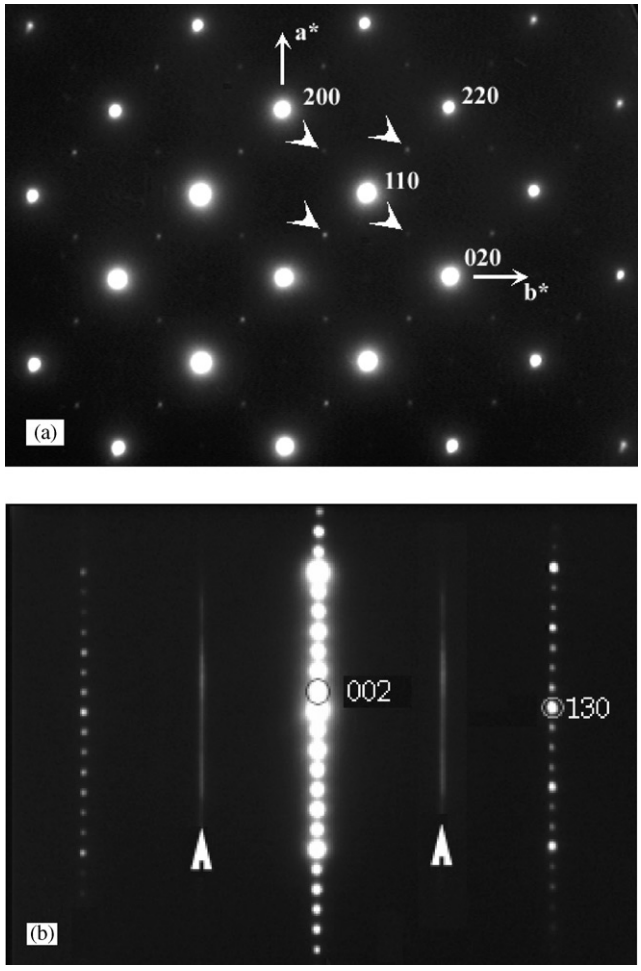

Fig. 5. (a) [001] and (b) [3$\bar{1}$0] ED pattern of $Sr_4FeMnO_6CO_3$ showing the extra reflections (white triangles). The patterns are indexed in the tetragonal subcell $I4/mmm$ with $a=a_p$ and $c \approx 28$ Å.

possibilities were considered concerning the configuration of the carbonate groups, a "flag" configuration observed for $Sr_2CuO_2CO_3$ [7] and $Hg_{0.5}Cr_{0.5}Sr_4Cu_2O_7CO_3$ [13] we will call flag's model (see Fig. 6a), a "coat hanger" configuration observed for $Sr_4FeCrO_6CO_3$ [6] called coat hanger's model (see Fig. 6b) and a mixture of flag and coat hanger configurations observed for $Sr_4Fe_2O_6CO_3$ [4] called mixed model. All these configurations were tested for $Sr_4FeMnO_6CO_3$ considering isotropic thermal displacements for all atoms. The best fits were obtained with flag's and mixed's models which led to very close agreement factors and χ^2 (Rwp = 3.99% and 4.05%, $\chi^2 = 2.71$ and 2.66, respectively) whereas for the coat hanger configuration Rwp = 5.32% and $\chi^2 = 4.73$. The two first models were considered for complete structural determination. The results are given in Table 2. An example of fitted experimental diffraction pattern is drawn in Fig. 7.

In both cases the fits are slightly improved with a partial occupation of carbon site by manganese ion, as confirmed by X-ray diffraction. The scattering lengths of Fe (0.945×10^{-12} cm) and of Mn (-0.373×10^{-12} cm) allow to make a difference between these two elements. In our case they showed without ambiguity that if carbon site is partially occupied by a foreign atom, this atom is manganese. To keep the ratio Fe/Mn = 1, this implies that in the mixed Fe–Mn site, the amount of Fe increases.

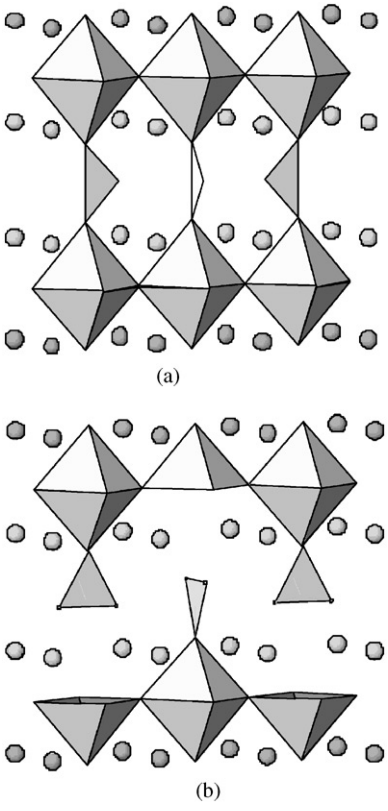

Fig. 6. (a) Structural model for flag's model and for coat hanger's model (b).

The main difference between the results of the two structural models is the U value of oxygens surrounding carbon which is twice as large in the flag model as in the mixed one (0.035 and 0.018 Å^2, respectively). This strongly suggests that the second model, which corresponds to a mixture of several configurations for the CO_3 groups, is the right one. It is the model which is considered in the continuation of this paper.

The interatomic distances are listed in Table 3. The environment of Fe/Mn atoms is characterized by four equatorial Fe/Mn–O(2) long bond distances close to 1.98 Å and one short Fe/Mn–O(1) bond distance close to 1.83 Å. Other oxygen atoms (O(3) and O(5)) sit at very large distances (2.67 and 3.06 Å) and cannot be considered as belonging to the transition metal polyhedron. Such a situation is very similar to that encountered in $Sr_4Fe_2O_6CO_3$ [4]. The angle between two opposite Fe/Mn–O(3) bonds (154.5(2)°) is slightly smaller than the Mn free sample (159.6°), showing that the introduction of manganese is accompanied by a slight displacement of the transition metals inside the pyramid.

Four possible configurations are possible for carbonate groups (Fig. 8). Among them, only two seems more realistic: the "coat hanger" configuration $(CO(3)O(4)_2$, Fig. 8a) and the flag configuration $(CO(5)_2O(6)$, Fig. 8d). They should be 90° rotated with regard to the c-axis from one position to each other to avoid too short O–O distances. In both configurations carbon exhibits one long and two short carbon–oxygen bonds and O–C–O angles are characterized by one large and two small angles (Table 3).

3.3.2. *Quantification of manganese on carbon site*

From refinements it appears that approximately 5% of the carbon site is occupied by manganese. Another way to estimate the percentage of transition metal on the carbon site is to determine the amount of unreacted strontium carbonate. This amount is 2.4(2) wt% for $x = 1$, according to the NPD data.

Considering the general reaction :

$$SrCO_3 + 3\ SrO + (1 - x/2)\ Fe_2O_3 + x/2\ Mn_2O_3 \rightarrow p\ SrCO_3 + t\ Sr_4(Fe_{2-x}Mn_x)_{1+y}(CO_3)_zO_q,$$

we can assume that each element is preserved because of the use of sealed tube for the synthesis. In this case, $t = (4 - p)/4$, leading to the general formula:

$$Sr_4(Fe_{2-x}Mn_x)_{(4/(4-p))}(CO_3)_{(4(1-p)/(4-p))}O_{(24/(4-p))}$$

and we can write as a function of x and y: $Sr_4(Fe_{2-x}Mn_x)_{1+y}(CO_3)_{1-3y}O_{6(1+y)}$. In the above writing, iron and manganese remain in the trivalent state as confirmed by XANES (see hereafter).

Table 2
Structural parameters of $Sr_4(Fe_{2-x}Mn_x)_{1+y}(CO_3)_{1-3y}O_{6(1+y)}$. The first line refers to mixed model and the second one (italic letters) refers to flag's model

Atom	Site	x	y	z	U (Å^2)	n
Sr(1)	4e	0.0	0.0	0.57229(8)		4
		0.0	*0.0*	*0.57237(10)*		*4*
Sr(2)	4e	0.0	0.0	0.70169(8)		4
		0.0	*0.0*	*0.70192(8)*		*4*
Fe/Mn	4e	0.0	0.0	0.14626(18)	0.000(1)	2.05 (2)/1.95 (2)
		0.0	*0.0*	*0.14628(20)*	*0.003(2)*	*2.04 (2)/1.96(2)*
C/Mn	2a	0.0	0.0	0.0		1.90(2)/0.10 (2)
		0.0	*0.0*	*0.0*		*1.92(2)/0.08(2)*
O(1)	4e	0.0	0.0	0.21092(12)		4
		0.0	*0.0*	*0.21112(14)*		*4*
O(2)	8 g	0.0	0.5	0.13083(6)		8
		0.0	*0.5*	*0.13102(8)*		*8*
O(3)	4e	0.0	0.0	0.0517(5)	0.018(2)*	1
		0.0	*0.0*	*0.0487(3)*	*0.035(2)***	*2*
O(4)	16n	0.273 (4)	0.0	0.0191(5)	0.018(2)*	2
		0.346 (4)	*0.0*	*0.0086(6)*	*0.035(2)***	*2*
O(5)	16n	0.136 (4)	0.0	0.0397(5)	0.018(2)*	2
		0.213 (5)	*0.0*	*0.0294(7)*	*0.035(2)***	*2*
O(6)	8i	0.376 (5)	0.0	0.0	0.018(2)*	1

Atom	U_{11}(Å^2)	U_{22} (Å^2)	U_{33} (Å^2)	Ueq (Å^2)
Sr(1)	0.0109(9)	$=U_{11}$	0.0076(14)	0.0097(10)
	0.0081(8)		*0.0085(14)*	*0.082(10)*
Sr(1)	0.0090(8)	$=U_{11}$	0.0071(14)	0.0083(10)
	0.0095(8)		*0.0040(14)*	*0.0077(10)*
C/Mn	0.0137(16)	$=U_{11}$	0.0174(25)	0.0149(19)
	0.0126(16)		*0.0160(24)*	*0.0137(18)*
O(1)	0.0091(8)	$=U_{11}$	0.0048(14)	0.0076(10)
	0.0101(8)		*0.0063(14)*	*0.089(10)*
O(2)	0.0077(10)	0.0057(10)	0.0165(14)	0.0100(11)
	0.0087(10)	*0.0069(10)*	*0.0145(14)*	*0.0100(11)*

*, **Refined with the same value.
a = 3.8569(2) Å, c = 28.272(2) Å; R_p = 3.26%, R_{wp} = 3.81%, χ^2 = 2.40, R_B = 4.12%; *a = 3.8570(2) Å, c = 28.272(2) Å; Rp = 3.19%, Rwp = 3.86%, χ^2 = 2.54, R_B = 4.13%.*
Between brackets are the e.s.d's multiplied by Berar's formula parameter.

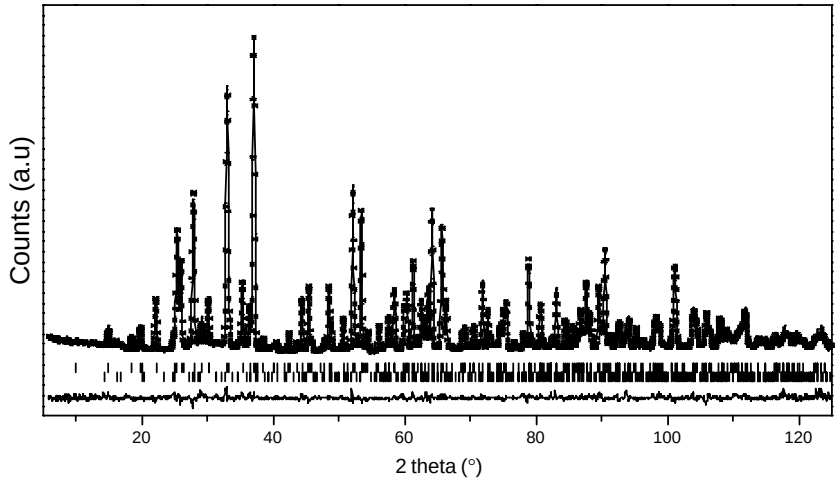

Fig. 7. Experimental (crosses), calculated and difference (solid lines) neutron powder diffraction pattern of $Sr_4FeMnO_6CO_3$ at the end of refinement. The vertical bars are the Bragg angle positions for the main phase (upper) and the impurity $SrCO_3$ (lower).

Table 3
Interatomic distances and angles (mixed model).

M – O	d (Å)	× n*	M –O	d (Å)	× n*
Sr(1)– O(2)	2.541(2)	× 4	Fe/Mn–O(1)	1.828(6)	× 1
O(3)	2.788(3)	× 1	O(2)	1.977(1)	× 4
O(4)	2.598(10)	× 1	O(3)	2.672(16)	× 0.25
O(5)	2.558(9)	× 1	O(5)	3.057(14)	× 0.5
O(6)	2.850(4)	× 1			
			C-O(3)	1.463(15)	× 0.5
Sr(2)– O(1)	2.471(4)	× 1	O(4)	1.184(14)	× 1
O(1)	2.740(1)	× 4	O(5)	1.239(14)	× 1
O(2)	2.781(2)	× 4	O(6)	1.452(20)	× 0.5
		O–C–O angles (deg)			
	O(4)–O(3)–O(4) triangle			O(5)–O(6)–O(5) triangle	
O(3)–C–O(4)	117.0(7)	× 2	O(5)–C–O(5)	130.1(9)	× 1
O'4)–C–O(4)	125.9(10)	× 1	O(5)–C–O(6)	115.0(6)	× 2

*The n values take into account the site occupancy.

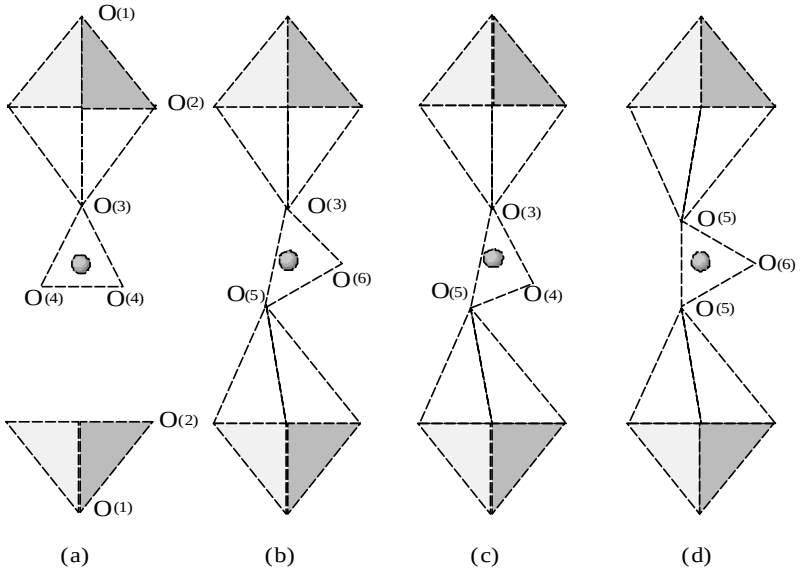

Fig. 8. Different possible geometries of CO_3 groups. The "coat-hanger" configuration (a) and the "flag" configuration (d) are the most probable.

Coming back to the $x=1$ sample, one obtains $p=0.1$ and $1+y=1.026$; consequently the amount of transition metal on the carbon site would be 0.052 ($2y$).

The same procedure was used to test other compositions from X-ray diffraction data. For the same sample, the amount of unreacted strontium carbonate calculated by the program was 2.3(2) wt%, i.e. a value very close to that obtained from neutron diffraction data. It showed that , in this case, the quantitative analysis of $SrCO_3$ in the mixtures can be attempted. The results are listed in Table 4 where they are compared to those obtained from EDS analyses on about 30 crystals for each composition and from refinements of the carbon site occupancy. In spite of some discrepancy in the results, in all cases the amount of transition metal (TM) on the carbon site increases when increasing x for $x>0.7$. It seems that there is no direct correlation between x and y. Assuming that the transition metal is preferably manganese, as it appears from the neutron diffraction study of the $x=1$ sample, the local formation of $n=3$ member of the RP series tends to brake the decrease of iron in the two outer TM–O layers.

3.3.3. *Xanes and Mössbauer spectroscopy*

XANES studies of nominal $Sr_4Fe_{2-x}Mn_xO_6CO_3$ samples with $x=0.5$, 1 and 1.5 were performed in order to determine the oxidation states and to confirm the coordination of the Fe and Mn species.

Iron K-edge: The Fe K-edge spectra of the three compositions mentioned above and of four reference oxides, Fe_2O_3, $Sr_4FeCrO_6CO_3$ and $Sr_4Fe_2O_6CO_3$ for Fe^{3+}, and $SrFeO_3$ for Fe^{4+} formal charges are shown in Fig. 9. The energy at midheight of the main absorption

Table 4
Number of transition metal atoms occupying the carbon site (2*y*), deduced from several analytical techniques : (a) from amount of unreacted $SrCO_3$ (USC), (b) from refinement of carbon site occupancy, (c) from EDS analysis

x	USC % ±0.4	*2y*		
		(a) ±.0.01	(b) ±0.02	(c) ±0.03
0.3	0.0	0.0	—	0.0
0.7	0.3	0.0	—	0.05
1.0	2.3	0.05	0.07	0.09
[a]	*2.4*	*0.05*	*0.05*	
1.3	8.3	0.19	0.16	0.20
1.5	12.4	0.29	0.32	0.30

[a] Neutron diffraction results (italic letters).

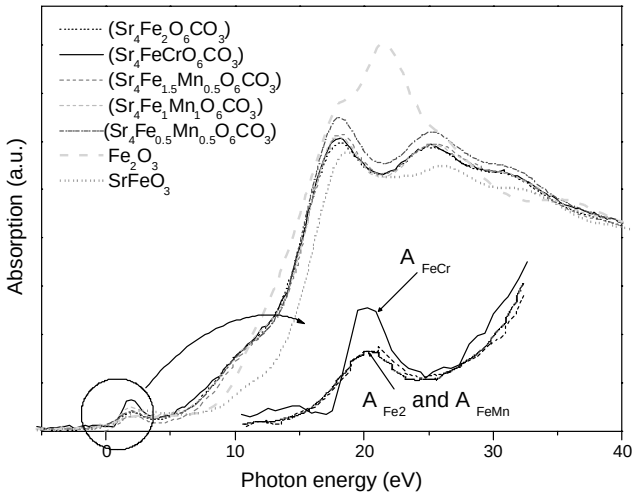

Fig. 9. XANES Normalized Fe K-edges at room temperature for iron references and for nominal compositions of $Sr_4Fe_{2-x}Mn_xO_6CO_3$, $x=0$, 0.5, 1 and 1.5.

jump (Table 5) allows the oxidation state to be estimated at +3 for the three compositions.

One can see that spectra of the three Fe/Mn samples are unchanged and identical to that of $Sr_4Fe_2O_6CO_3$, contrary to that of $Sr_4FeCrO_6CO_3$ for which the prepeak labeled A_{Cr} is more intense. This suggests that in the mixed Mn/Fe oxycarbonates, the iron environment should be the same as in the free manganese oxycarbonate and different from that in the mixed Cr/Fe oxycarbonate in which it is exclusively pyramidal [6].

To check this hypothesis about the iron coordination, the Mössbauer spectrum of $Sr_4FeMnO_6CO_3$ (Fig. 10) was registered at room temperature and compared to that of $Sr_4FeCrO_6CO_3$. Both spectra show the existence of pure quadripolar electric interactions at 293 K and IS values corresponding to trivalent charges. Contrary to the mixed Cr/Fe fit [6], the $Sr_4FeMnO_6CO_3$ one evidences two iron sites (96–4%), which could be explained by the presence of $n=3$ RP member in the matrix. The quadrupole splitting (QS) of the two fits

Table 5
Formal charge (FC), d_{M-O}, energy of main jump midheight (EMJM) at Mn K-edge and Fe K-edge for references and "$Sr_4Fe_{1.5}Mn_{0.5}O_6CO_3$", "$Sr_4FeMnO_6CO_3$" and "$Sr_4Fe_{0.5}Mn_{1.5}O_6CO_3$"

Compounds	FC	d_{M-O} (Å)	EMJM(eV) ± 0.3 eV
Mn_2O_3		1.86 × 2	
	+3	1.92 × 2	16.2
		1.88 × 1	
		1.91 × 1	
"$Sr_4Fe_{1.5}Mn_{0.5}O_6CO_3$"		1.88 × 1	
	+3	1.97 × 4	16.3
		2.64 × 0.25	
		2.97 × 0.5	
"$Sr_4FeMnO_6CO_3$"		1.82 × 1	
		1.97 × 4	
	+3	2.67 × 0.25	16.4
		3.05 × 0.5	
"$Sr_4Fe_{0.5}Mn_{1.5}O_6CO_3$"		1.80 × 1	
		1.97 × 4	
	+3	2.70 × 0.25	16.4
		3.15 × 0.5	
MnO_2	+4	1.87 × 4	18.8
		1.89 × 2	
Fe_2O_3		1.94 × 3	
	+3	2.11 × 3	13.6
"$Sr_4FeCrO_6CO_3$"		1.97 × 4	
	+3	1.85 × 1	13.9
"$Sr_4Fe_2O_6CO_3$"		1.97 × 4	
	+3	1.90 × 1	13.9
		2.60 × 0.25	
		2.94 × 0.5	
"$Sr_4Fe_{1.5}Mn_{0.5}O_6CO_3$"		1.88 × 1	
	+3	1.97 × 4	13.7
		2.64 × 0.25	
		2.97 × 0.5	
"$Sr_4Fe_1Mn_1O_6CO_3$"		1.82 × 1	
	+3	1.97 × 4	13.9
		2.67 × 0.25	
		3.05 × 0.5	
"$Sr_4Fe_{0.5}Mn_{1.5}O_6CO_3$"		1.80 × 1	
	+3	1.97 × 4	13.8
		2.70 × 0.25	
		3.15 × 0.5	
$SrFeO_3$	+4	1.92 × 4	15.1
		1.98 × 2	

(0.58 for $Sr_4FeMnO_6CO_3$ and 0.66 for $Sr_4FeCrO_6CO_3$) is consistent with a Fe^{3+} polyhedron more symmetric in the mixed Mn/Fe compound than in Fe/Cr one. In the former, in addition to the five nearest oxygen atoms, oxygens are found at 3.07 and 2.67 Å from Mn/Fe whereas in the latter they sit at 3.73 Å from Cr/Fe.

Manganese K-edge: The Mn K-edge of the three mixed Fe/Mn oxycarbonates under consideration and of two reference oxides Mn_2O_3 (for Mn^{3+}) and MnO_2 (for Mn^{4+}) are shown in Fig. 11. Note that the three spectra are identical and the energy at midheight of the main absorption jump allows the oxidation states to be fixed to 3+. The relative intensities of the prepeaks due to a strong hybridization of Mn(3*d*)–O(2*p*)–Mn(4*p*) orbitals

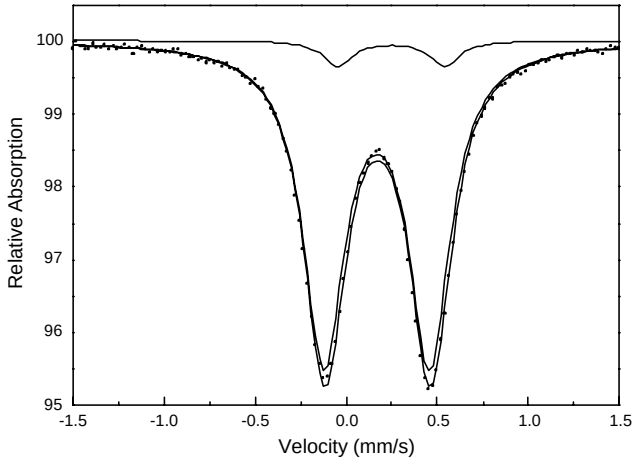

Fig. 10. Mössbauer spectrum of $Sr_4FeMnO_6CO_3$ reported at room temperature.

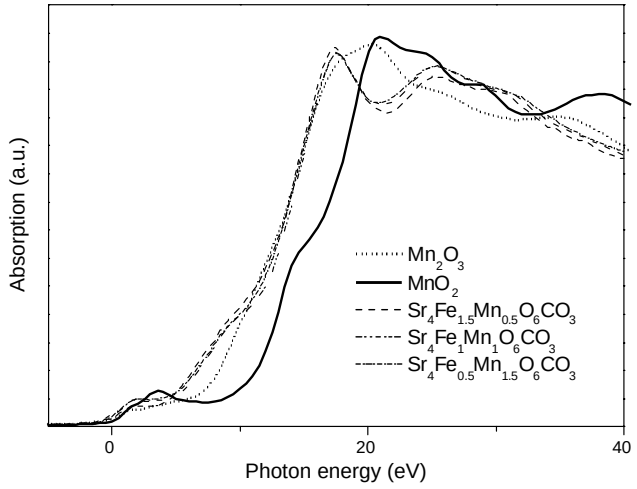

Fig. 11. XANES Normalized Mn K-edges at room temperature for manganese references and for nominal compositions of $Sr_4Fe_{2-x}Mn_xO_6CO_3$, $x=0$, 0.5, 1 and 1.5.

indicate a non-centrosymmetric environment like non-regular octahedron, which is compatible with the structural results.

Whatever x (0.5, 1, 1.5), one can see the similarity between the Fe and Mn K-edge spectra. This is in perfect agreement with the neutron diffraction results for which the iron and manganese atoms are distributed over the same crystallographic site, implying the same environment. The peaks labeled B could be correlated to the 1*s*–4*p* transition corresponding to non-bonding orbitals pointing towards long M–O distances, whereas the peaks labeled C are correlated to the 1*s*–4*p* transition corresponding to bonding orbitals pointing towards the short M–O distances.

In the limit of the technique accuracy we can admit that there is no evolution of the oxidation state of the two species Fe and Mn in the series $Sr_4(Fe_{2-x}Mn_x)_{1+y}$

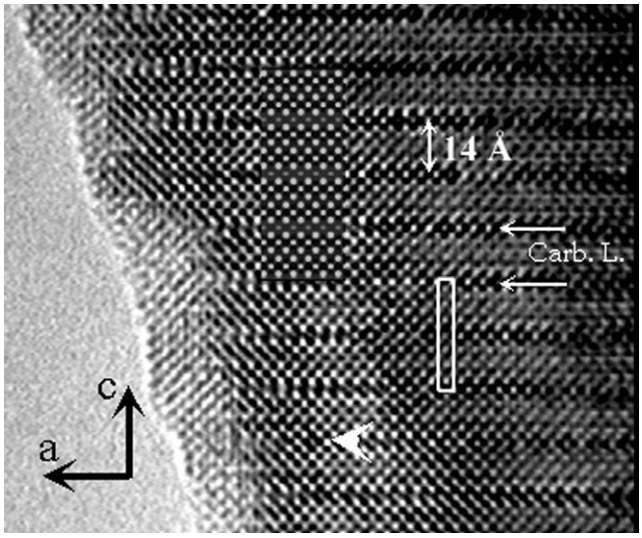

Fig. 12. [010] HREM of $Sr_4Fe_{0.5}Mn_{1.5}O_6CO_3$, where the carbonate rows (see small white arrows) and the rock salt layers appear as bright dots. The presence of manganese atoms in carbonate rows are pointed out with white triangles.

$(CO_3)_{1-3y}O_{6(1+y)}$ (with $0\leqslant x\leqslant 1.5$ and $0\leqslant y\leqslant 0.15$). This result is consistent with syntheses in closed atmosphere.

3.4. Nanostructural state

3.4.1. HREM study: organization of the carbonate layers

One of the purposes of this study is to understand the origin of the extra reflections and disorder phenomena in our compound. The nature and the stacking mode of different layers are easily visible by viewing the crystals along [0 1 0]. This is illustrated in the [0 1 0] HREM image of the $x=1.5$ sample displayed in Fig. 12 where the carbonate layers (white arrows) are regularly spaced by about 14 Å along $\vec{c}$. It is recorded for a focus value close to −55 nm, i.e. the bright dots are correlated to the high electron density zones. The experimental contrast fits with the theoretical one (inset) calculated for a crystal thickness of 25 Å and a focus value of –55 nm, using the refined position parameters (Table 2), the row of small gray dots is correlated to the carbonate layer. The HREM study of numerous crystallites of $x=1$ and 1.5 shows that the stacking mode of different layers is highly regular, without any intergrowth defects. However, local variations of the contrast in the carbonate rows (see white triangle) where the gray dots are replaced by bright ones, appear for [0 1 0] HREM images. These defects are running over a few nanometers long but are never periodically established, even over a short-range distance. These phenomena are directly correlated to the presence of manganese atoms on the carbon site, implying the presence of intergrowth domains (RP3) in the matrix.

The last step was to characterize the origin of the superstructure. The best orientation to observe these phenomena is [3 $\bar{1}$ 0]. The image ($Sr_4Fe_2O_6CO_3$) displayed in Fig. 13, shows that superstucture is only visible at the level of the carbonate layers (see white arrows). The contrast consists in alternating bright spots spaced by about 2.5 Å ($2d_{3\bar{1}0}$, along 3$\bar{1}$0]). In the adjacent carbonate rows, this effect is simply translated by $\vec{c}$ or suffers an additional shifting by d_{130}, involving a local centered contrast (see black arrows). Every carbonate layer exhibits this superstructure but no ordering is observed, along $\vec{c}$, in the relative arrangement of these bright dots, generating the streaks along $\vec{c}$. This feature previously observed in other layered carbonates [14] is correlated to the organization of the carbonate groups which rotate along c^* and will be detailed elsewhere. Note that the positions of the bright dots are not static and the contrast "moves" under electron beam diffraction. This effect could be correlated to the rather easy rotation of the carbonate groups under irradiation.

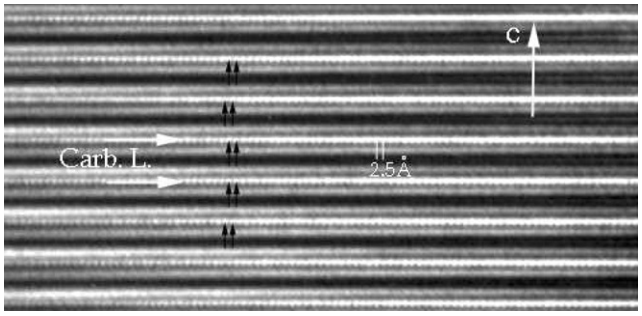

Fig. 13. [3$\bar{1}$0] HREM of $Sr_4Fe_2O_6CO_3$ showing that the short-range ordering correlated with the extra reflection in the ED patterns (Fig. 5) arises at the carbonate layers level (white arrows), that one appears as rows of bright dots (black arrows).

In the light of this study, the specific organization of carbonate groups within a layer is at least partly responsible for the orthorhombic distortion. The latter is clearly visible (for specific orientation) in the ED study, but cannot be taken into account in the average structure determination, owing to "disorder" phenomena along c^*. The organization of carbonate groups which rotate along c is not regular in the successive layers.

3.5. Magnetism

The magnetic susceptibility measurements performed in the range 5–300 K in an applied field of 3000 G show, for $Sr_4FeMnO_6CO_3$, a progressive (χ-$\chi_{paramagnetic}$) decrease starting from 140 K and down to 35 K (Fig. 14). Such a curve shape is reminiscent of 2D antiferromagnetism. The linear part of χ_M^{-1} (inset of Fig. 14) was fitted with the Curie–Weiss law $\chi = \chi_0 + C/(T-\theta p)$ (C is the Curie constant, θp is the paramagnetic Curie temperature and χ_0 is the temperature-independent susceptibility). The important negative θp value (−650 K) is characteristic of strong antiferromagnetic interactions in this compound. From the Curie constant, an effective magnetic moment value (μ_{eff}) of 7.75 μ_B/mol is obtained. This value is close to the expected one calculated by considering Fe^{3+} and Mn^{3+} in high spin configuration ($\mu_{calc} = 7.68\ \mu_B$).

The magnetic behavior of the $x = 1.5$ sample is different from that of $Sr_4FeMnO_6CO_3$. The magnetic

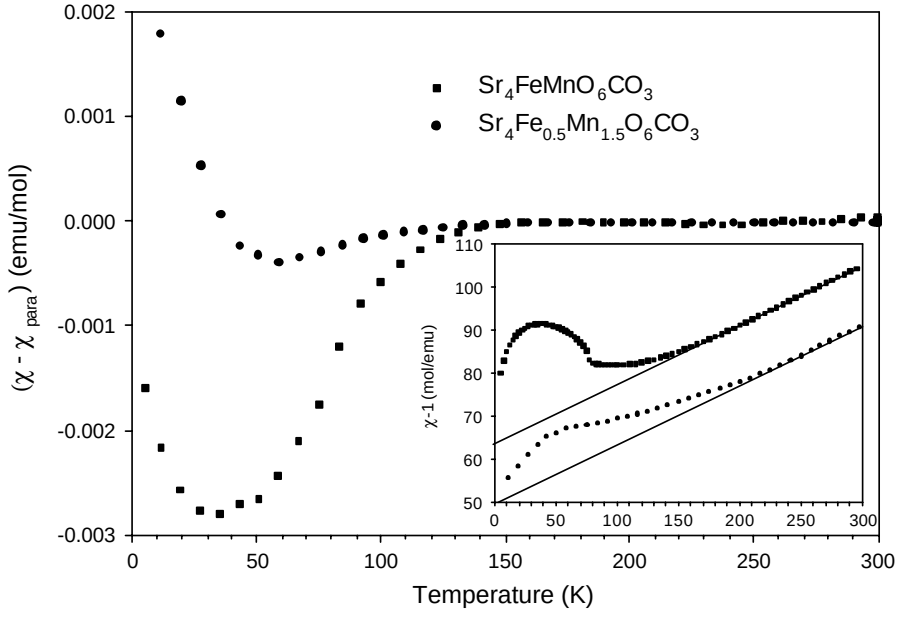

Fig. 14. (χ-χ_{para})(T) curves of $Sr_4FeMnO_6CO_3$ and $Sr_4Fe_{0.5}Mn_{1.5}O_6CO_3$, obtained from the ZFC $M(T)$ curves recorded at 3000G. Inset: χ^{-1} (T) curves of $Sr_4FeMnO_6CO_3$ and $Sr_4Fe_{0.5}Mn_{1.5}O_6CO_3$ (solid lines are the fit).

susceptibility measurements performed in the range 5–300 K in an applied field of 3000 G revealed a behavior relatively similar to that of the $n=3$ member $Sr_4Mn_2FeO_{9.8}$ [15] of the RP family, which could be explained by the presence of the latter in the form of intergrowth defects or domains, in the matrix. The Curie–Weiss fit performed (tacking into account the weight contribution of $SrCO_3$) in the linear part of χ_M^{-1} leads to a negative θp value (-500 K) and an effective magnetic moment value (μ_{eff}) of 7.5 μ_B ($\mu_{calc}=7.3\,\mu_B$ considering Fe^{3+} and Mn^{3+} in high spin configuration).

The interaction between nearest neighbors, Fe^{3+}/Fe^{+3}, Mn^{3+}/Mn^{3+} cation pairs, is unambiguously antiferromagnetic. It has been predicted that the superexchange between a $3d^5$ and a $3d^4$ ion should be antiferromagnetic through the π orbitals and ferromagnetic through the σ orbitals. The majority of the magnetic interactions being antiferromagnetic it is thus reasonable to observe an antiferromagnetic state for these compositions.

The Mn for Fe substitution seems to suppress the ferromagnetic interactions which exist in the $Sr_4Fe_2O_6CO_3$ oxycarbonate: Yamaura *et al.* [4] report that this compound exhibits a three-dimensional magnetic ordering transition at 361 K characterized by an antiferromagnetic order within the $FeO_2/SrO/SrO/FeO_2$ blocks and a ferromagnetic order between the blocks.

4. Conclusion

In conclusion, the possibility for trivalent manganese to partially substitute for trivalent iron in layered oxycarbonates has been shown. It is remarkable that the mode of connection of the triangular CO_3 groups differs from that observed in $Sr_4FeCrO_6CO_3$, by the coexistence of two configurations called "flag" and "coat hanger". The ability of manganese to sit for a small part on the carbonate sites must also be emphasized. The antiferromagnetic behavior of this phase, different from that of the free manganese compound, confirms that manganese suppresses the ferromagnetic interactions that exist in $Sr_4Fe_2O_6CO_3$.

References

[1] J.C. Bednorz, K. Müller, Z. Phys. B 64 (1986) 189.
[2] Y. Moritomo, A. Asamitsu, H. Kuwhara, Y. Tokura, Nature. 380 (1996) 141.
[3] S.R. Ruddlesden, P. Popper, Acta Crystallogr. 10 (1957) 538; S.R. Ruddlesden, P. Popper 11 (1958) 54.
[4] K. Yamaura, O. Huang, J.W. Lynn, R.W. Erwin, R.J. Cava, J. Solid State Chem. 152 (2000) 374.
[5] Y. Bréard, C. Michel, M. Hervieu, B. Raveau, J. Mater. Chem. 10 (2000) 1043.
[6] Y. Bréard, C. Michel, M. Hervieu, B. Raveau, N. NGuyen, A. Ducouret, F. Studer, E. Suard, Chem. Mat. 13 (2001) 2423.
[7] T.G.N. Babu, D.J. Fish, C. Greaves, J. Mater. Chem. 1 (1991) 677.
[8] B. Raveau, M. Huvé, A. Maignan, M. Hervieu, C. Michel, B. Domengès, C. Martin, Physica C 209 (1993) 350.
[9] V. Caignaert, B. Domenges, B. Raveau, J. Solid State Chem. 120 (1995) 279.
[10] D. Pelloquin, M. Hervieu, C. Michel, B. Raveau, J. Solid State Chem. 134 (1997) 395.
[11] J. Rodriguez Carvajal, Collected Abstract of Satellite Meeting on Powder Diffraction of XVth. Congr. Int. Union. Crystallographic. Toulouse, 1990, p. 127.
[12] L. Er-Rakho, C. Michel, B. Raveau, J. Solid State Chem. 73 (1988) 514.
[13] S. Malo, C. Michel, D. Pelloquin, M. Hervieu, O. Toulemonde, B. Raveau, Physica C 304 (1998) 213.
[14] O. Milat, G. VanTendeloo, S. Amelinks, T.G.N. Babu, C. Greaves, J. Solid State Chem. 97 (1992) 4005.
[15] P.D. Battle, W.R. Brandford, A. Mihut, M.J. Rosseinsky, J. Singleton, J. Sloan, L.E. Spring, J.F. Vente, Chem. Mater. 11 (1999) 674.